Electron-impact excitation of argon: Cross sections of interest in plasma modeling

R. K. Gangwar,[1] L. Sharma,[2] R. Srivastava,[1] and A. D. Stauffer[3]
[1]*Department of Physics, Indian Institute of Technology, Roorkee 247667, India*
[2]*Physikalisches Institut, Universität Heidelberg, D-69120 Heidelberg, Germany, and GSI Helmholtzzentrum für Schwerionenforschung GmbH, Planckstrasse 1, D-64291 Darmstadt, Germany*
[3]*Department of Physics and Astronomy, York University, Toronto M3J 1P3, Canada*
(Received 26 January 2010; published 24 May 2010)

We used the relativistic distorted-wave approximation to calculate the excitation of Ar from its ground-state $3p^6$ configuration to the higher lying fine-structure levels of the $3p^5 3d$, $3p^5 5s$, and $3p^5 5p$ manifolds. The calculation has been performed with relativistic Dirac-Fock multiconfiguration wave functions for the ground and excited states. Results for the differential and integrated cross sections are obtained at energies in the range up to 100 eV, and these are compared with available experimental measurements and earlier theoretical nonrelativistic distorted-wave and *R*-matrix calculations. Analytic fits to our integrated cross sections are provided.

DOI: 10.1103/PhysRevA.81.052707 PACS number(s): 34.80.Dp

I. INTRODUCTION

Recently, attention has focused on the study of electron-impact excitation of inert gas atoms because the excitation cross sections for these atoms are important in plasma modeling applications. Optical emission diagnostics of rare gas plasmas are widely used in laboratory and astrophysical plasma studies and also in numerous industrial applications [1]. Basic parameters of the plasma such as electron temperature and electronic density, as well as information about the plasma constituents, can be obtained by collisional radiative models (CRMs) [2]. These models require accurate electron-excitation cross-sectional data from both the ground and excited states of the rare gas atoms, and thus there is a need for such cross-sectional data over a wide range of projectile energies and for transitions between different fine-structure levels.

There have been many theoretical and experimental investigations of electron collisions with rare gases using both differential cross sections (DCSs) and integrated cross sections (ICSs) [1,3]. Most of these studies have considered excitation only from the ground (np^6) state to the excited $np^5(n+1)s$ and $np^5(n+1)p$ states in Ne ($n=2$), Ar ($n=3$), Kr ($n=4$), and Xe ($n=5$). Previously, we successfully applied the relativistic distorted-wave (RDW) method to calculate electron-impact excitation of the various inert gases from their ground and metastable states [4,5]. Our RDW method is a completely relativistic treatment of electron scattering using the Dirac equations to calculate the wave functions of both the initial and final bound target states as well as for the scattered electron [6].

However, there are several more fine-structure transitions for which excitation cross sections are needed for plasma modeling. In the present work, we calculated excitation cross sections for the excitation of the $3p^5 3d$, $3p^5 5s$, and $3p^5 5p$ manifolds from the ground level of the Ar atom. Here we report calculations of the ICSs for all these excitations as well as DCS results for $3p^5 3d$ and $3p^5 5s$ transitions and compare them to earlier calculations and measurements.

There have been three sets of measurements for these transitions. Chutjian and Cartwright [7] have measured DCSs for the excitation of the $3p^5 3d$ and $3p^5 5s$ fine-structure levels (not all of which were resolved) and derived ICSs from their extrapolated data. Chilton and Lin [8] reported ICSs for the excitation of these same levels when the total angular momentum J is not equal to 1 (since the levels with $J=1$ can decay radiatively to the ground state). Weber *et al.* [9] measured the optical emission spectrum of the $3p^5 5p$ levels and derived apparent ICS data from their measurements, which were not corrected for cascade. Bubelev and Grum-Grzhimailo [10] carried out theoretical distorted-wave calculations for the ICSs of the excitation of the $3p^5 3d$ and $3p^5 5s$ levels, and Madison *et al.* [11] reported similar results for the $3p^5 3d$ levels using both distorted-wave Born and *R*-matrix approximations. Bartschat (private communication) has done *R*-matrix calculations of the excitation of the $3p^5 5s$ levels based on the method given in Bartschat and Zeman [12].

II. THEORY

A. Wave functions

The ground state of argon has the configuration $1s^2 2s^2 2\bar{p}^2 2p^4 3s^2 3\bar{p}^2 3p^4$ in *j*-*j* coupling, where $\bar{p}$ represents a p orbital with total angular momentum (orbital plus spin) $j=1/2$ and p has $j=3/2$. It has even parity and $J=0$. The $3p^5 3d$ and $3p^5 5s$ manifolds have odd parity and consist of twelve and four fine-structure levels, respectively. These are designated as $3d_k$ ($k=1$, 12) and $2s_k$ ($k=2$, 5) in order of decreasing energy. We have carried out a multiconfiguration calculation for the wave functions of these levels using the GRASP92 program of Parpia *et al.* [13]. We included the configurations where one of the valence p orbitals is excited to one of $4s$, $5s$, $3\bar{d}$, or $3d$ orbitals. The coefficient of the configurations in each of these levels is given in Table I. Our calculations give an inverted order to the $3d_2$ and $3d_3$ levels, which have almost identical energies. We have carried out similar calculations for the $3p^5 5p$ manifold, which has even parity and ten fine-structure levels designated as $3p_k$ ($k=1$, 10). For these levels, the configurations include the excited $4\bar{p}$, $4p$, $5\bar{p}$, and $5p$ orbitals, and the coefficients are given in Table II. Again, we have an inversion of the $3p_2$ and $3p_3$ levels, but we use our energy ordering of these levels

TABLE I. Coefficients of various configurations in the multiconfiguration wave functions of the $3p^5 3d$ and $3p^5 5s$ levels of Ar.

Configurations	$3\bar{p}^2 3p^4$	$3\bar{p}^2 3p^3 4s$	$3\bar{p}3p^4 4s$	$3\bar{p}^2 3p^3 3\bar{d}$	$3\bar{p}^2 3p^3 3d$	$3\bar{p}3p^4 3\bar{d}$	$3\bar{p}3p^4 3d$	$3\bar{p}^2 3p^3 5s$	$3\bar{p}3p^4 5s$
$J = 0$ levels									
$1p_0$	1.0	–	–	–	–	–	–	–	–
$3d_{12}$		–	0.0513	0.9924	–	–	–	–	−0.1118
$2s_3$	–	–	0.0561	0.1089	–	–	–	–	0.9925
$J = 1$ levels									
$3d_{11}$	–	−0.0117	0.0434	0.7976	−0.5128	0.2053	–	0.2130	0.1065
$3d_5$	–	−0.0063	0.0087	0.5711	0.7123	−0.3947	–	0.0094	−0.1021
$2s_4$	–	0.0787	−0.0034	−0.1789	0.1314	−0.0233	–	0.9674	0.0895
$2s_2$	–	−0.0236	0.0699	−0.0101	0.1100	−0.0709	–	−0.1073	0.9827
$3d_1$	–	−0.0278	0.0116	0.0626	0.4455	0.8921	–	−0.0261	0.0108
$J = 2$ levels									
$3d_{10}$	–	−0.0051	–	−0.2892	0.6659	−0.0568	0.2778	0.6265	–
$2s_5$	–	0.0675	–	0.2401	−0.5556	0.0332	−0.1604	0.7761	
$3d_7$	–	0.0002	–	0.8819	0.3825	−0.2697	−0.0561	0.0009	–
$3d_4$	–	−0.0001	–	0.2532	0.1086	0.9411	0.1962	−0.0003	–
$3d_3$	–	−0.0230	–	0.1289	−0.2976	0.1930	0.9243	−0.0516	–
$J = 3$ levels									
$3d_8$	–	–	–	0.9896	0.0449	–	0.1364	–	–
$3d_6$	–	–	–	−0.0204	0.9842	–	−0.1760	–	–
$3d_2$	–	–	–	−0.1421	0.1714	–	0.9749	–	–
$J = 4$ levels									
$3d_9$	–	–	–	–	1.0	–	–	–	–

because it is the same as used by Weber *et al.* [9]. There are two possible angular momentum states of the $3p^5$ core, $j = 1/2$ and $3/2$, and in almost all cases one of these core states is dominant, representing more than 90% of the configurations. In particular, the domination of one core state is stronger for the $3p^5 5p$ levels than was the case for the $3p^5 4p$ levels [5]. This indicates that *j-j* coupling is more appropriate than *LS* coupling as electrostatic and spin-orbit interactions for this system are comparable.

In the calculations of electron-impact excitation, the most important parameter for the quality of the wave functions is the dipole oscillator strength for transitions between the initial and final states, as was shown by an investigation of transition probabilities of Xe atoms by Dasgupta *et al.* [14]. Only excited levels with odd parity and $J = 1$ are connected to the ground state by an allowed transition and hence give rise to a dipole oscillator strength. Where applicable, measured values in the National Institute for Standards and Technology (NIST) database [15] are compared to our results in Table III. Our values for the transitions to the $3d$ levels differ from the experimental measurements by about 50%, whereas the ones for the $5s$ levels are in much closer agreement.

TABLE II. Coefficients of the various configurations in the multiconfiguration wave functions of the $3p^5 5p$ levels of Ar.

Configuration	$3\bar{p}^2 3p^4$	$3\bar{p}^2 3p^3 4\bar{p}$	$3\bar{p}3p^4 4\bar{p}$	$3\bar{p}^2 3p^3 4p$	$3\bar{p}3p^4 4p$	$3\bar{p}^2 3p^3 5\bar{p}$	$3\bar{p}3p^4 5\bar{p}$	$3\bar{p}^2 3p^3 5p$	$3\bar{p}3p^4 5p$
$J = 0$ levels									
$1p_0$	1.0	–	–	–	–	–	–	–	–
$3p_5$	–	–	0.0628	0.1210	–	–	−0.6808	0.7197	–
$3p_1$	–	–	0.2472	0.3048	–	–	0.7034	0.5926	–
$J = 1$ levels									
$3p_{10}$	–	0.0385	0.0223	−0.0435	−0.0641	0.6609	−0.0624	0.7209	0.1775
$3p_7$	–	0.0142	0.0239	0.0116	0.0076	0.7338	−0.0916	0.6718	−0.0290
$3p_4$	–	0.0133	0.0139	0.0139	−0.0050	0.0661	0.9502	0.0701	0.2955
$3p_2$	–	0.0267	−0.0005	−0.0287	−0.0004	0.1293	−0.2900	−0.1404	0.9370
$J = 2$ levels									
$3p_8$	–	−0.0057	–	−0.0004	−0.0243	0.9783	–	0.1915	0.0752
$3p_6$	–	−0.0038	–	0.0240	0.0111	−0.1881	–	0.9806	−0.0479
$3p_3$	–	−0.0187	–	0.0057	−0.0021	−0.0831	–	0.0326	0.9958
$J = 3$ levels									
$3p_9$	–	–	–	−0.0255	–	–	–	0.999 7	–

TABLE III. Dipole oscillator strength for transition in the Ar: NIST, values from NIST database, and GRASP, present calculation.

States	NIST	GRASP
$3d_5$ $(J=1)$	9.32×10^{-2}	5.45×10^{-2}
$3d_1$ $(J=1)$	0.106	0.164
$2s_4$ $(J=1)$	2.7×10^{-2}	2.41×10^{-2}
$2s_2$ $(J=1)$	1.19×10^{-2}	9.83×10^{-3}

B. *T* matrices

In a distorted-wave approximation, the T matrix for electron-impact excitation of an atom having N electrons can be written as [6]

$$T_{a\to b}^{\mathrm{RDW}} = \langle X_b^-(1,2,\ldots,N+1)|V - U_b(N+1)|AX_a^+(1,2,\ldots,N+1)\rangle, \quad (1)$$

where V is the projectile electron-atom interaction potential. The distortion potential U_b is taken to be a function of only the radial coordinates of the projectile electron, r_{N+1}. We choose U_b to be the spherically averaged static potential of the excited state of the atom, which is the choice shown to yield most consistent results in the distorted-wave approximation. The wave functions $X_{a(b)}^{+(-)}$ in the initial state a and final state b are represented as a product of a *j-j* coupled multiconfiguration Dirac-Fock wave function $\Phi_{a(b)}(1,2,\ldots,N)$ with total angular momentum $J_{a(b)}$ for the target atom and a relativistic distorted wave for the projectile electron, which is the solution of a free-particle Dirac equation with the distortion potential U_b. Here, + indicates an outgoing wave, whereas – denotes an incoming wave. A is the antisymmetrization operator to account for exchange between the incident electron and the bound target electron.

The differential cross section is then given by

$$\frac{d\sigma}{d\Omega} = (2\pi)^4 \frac{k_b}{k_a} \left|T_{a\to b}^{\mathrm{RDW}}\right|^2, \quad (2)$$

where $k_{a(b)}$ is the momentum of the scattering electron in the initial (final) channel. The integrated cross section is obtained from (2) by integrating the DCS over all scattering angles.

Because the initial state a is the closed-shell ground state of Ar, we have $J_a = 0$. According to the angular momentum coupling of the final state, our expression for the direct term of the T matrix is nonzero only if J_b is odd for the odd parity ($3d$ and $5s$) states, whereas J_b must be even for the even parity ($5p$) state. In the other cases, only the exchange terms of the T matrix contribute to the cross sections. For exchange transitions, the ICSs drop off more rapidly with energy than those for which the direct term is nonzero. Generally, the DCSs for exchange transitions are relatively flat in the forward scattering region, whereas the direct transitions show a highly peaked DCS in this region.

For transitions for which the direct term is nonzero, the J_b value indicates the multipole moment of the interelectronic interaction which gives rise to this term. For the odd parity levels, the transitions to the ones with total angular momentum $J_b = 1$ are (optically allowed) dipole transitions and are expected to fall off more slowly with increasing impact energy than the other transitions. In the other cases, for both even and odd parity levels, as the J_b value becomes larger, the expected decrease in cross sections becomes faster as the energy increases.

III. RESULTS

A. Integrated cross sections

We show our ICS as a function of incident electron energy for the excitation of the $3d$ levels in Fig. 1. These are compared with the measurements of Chilton and Lin [8] and those derived from the measurements of Chutjian and Cartwright [7], as well as the theoretical values of Bubelev and Grum-Grzhimailo [10] and Madison *et al.* [11]. We only include the RM-SS (R-matrix calculation using atomic wave functions from the SUPERSTRUCTURE computer code) results and DW1 (semirelativistic distorted-wave method with unitarized S matrix) results from the latter paper. The RM-SS results give better agreement with the experimental measurements than the RM-CIV3 (R-matrix calculation using atomic wave functions from the CIV3 computer code) results, and the DW2 (nonunitarized semirelativistic distorted-wave method) results agreed well with the corresponding RM results at intermediate energies. The DW1 calculations include unitarization of the scattering matrix, which improves the cross sections near threshold.

In general, all theories have the expected behavior, as explained previously. The cross sections for the transitions to the $J_b = 1$ levels decrease slowly as the energy increases, whereas those with $J_b = 3$ fall off more rapidly by approximately an order of magnitude at 100 eV. Transitions to levels with even values of J_b have comparable values to the allowed transitions for energies around 20 eV but fall by two orders of magnitude at energies around 100 eV. The various theoretical results have similar shapes, though there is some variation in magnitude, in many cases by approximately a factor of two but in some cases by as much as an order of magnitude. The exception is the excitation of the $3d_{11}$ level, which from its J_b value of unity is expected to behave like an allowed dipole transition. However, the present RDW calculation and RM-SS results of Madison *et al.* [11] show that it behaves like a forbidden transition with odd J_b value. Chilton and Lin [8] note this behavior in their optical emission cross section. They report a configuration interaction calculation for this state in *LS* coupling which yields a very small coefficient for the singlet component of this level, and thus the dominant contribution comes from the triplet (forbidden) components. The DW1 results of Madison *et al.* [11] and the results of Bubelev and Grum-Grzhimailo [10] show a less rapid decrease, more typical of a level with $J_b = 3$. As Madison *et al.* [11] indicate, accurate wave functions are necessary to get the correct behavior of the cross section for this particular level.

Neither of the two experimental studies provides a direct measurement of the ICS. Chilton and Lin [8] measured the optical emission cross sections from the excited states. To obtain the direct excitation cross section requires correction for cascade contributions to the excited level as well as accurate knowledge of branching ratios for radiative decay. Chutjian and Cartwright [7] measured the DCS over the angular range of 10–140 deg. In order to obtain the ICS, the DCS were extrapolated to cover the complete angular range. Generally,

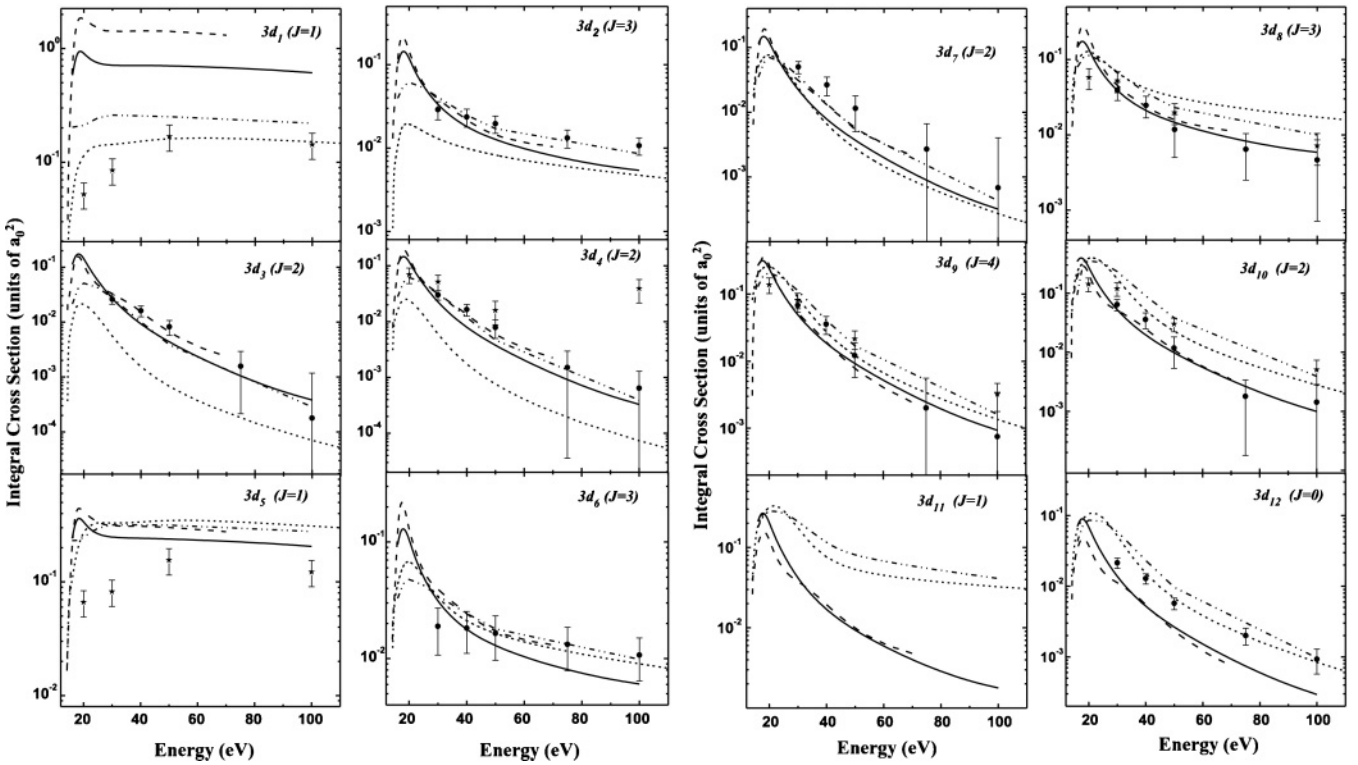

FIG. 1. Integrated cross sections in units of a_0^2 (where a_0 is the Bohr radius) for excitation of the $3p^5 3d$ levels: solid line, present RDW calculations; dashed line, RM-SS calculation of Madison *et al.* [11]; dotted line, unitarized distorted-wave (DW1) results of Madison *et al.* [11]; dashed-double dotted line, theoretical calculations of Bubelev *et al.* [10]; filled circles, experimental measurements of Chilton *et al.* [8]; stars, experimental measurements of Chutjian *et al.* [7].

the two sets of experimental ICSs do not agree with one another. Overall, the results of Chilton and Lin agree better with the theoretical calculations, but no theoretical results are consistently in good agreement with these data. Nevertheless, the analysis of the cross sections in terms of the J_b values of the excited levels, which is given above, is confirmed by these latter measurements.

Figure 2 shows the ICS for the excitation of the four fine-structure levels of the $3p^5 5s$ manifold. Our present RDW results are compared with the theoretical calculations of Bartschat (private communication) and Bubelev and Grum-Grzhimailo [10] as well as the experimental data of Chilton and Lin [8]. All of the theoretical results are quite similar, except for the excitation of the $2s_2$ level, where there is considerable difference in magnitude though general agreement in shape. Again, the behavior as a function of J_b is as expected. The results of Chilton and Lin [8] for the $2s_3$ and $2s_5$ transitions are substantially greater than the calculations, although they have a similar dependence on energy. There are no individual experimental cross-sectional measurements for the $2s_2$, $2s_4$, and $3d_{11}$ levels. However, Chutjian and Cartwright [7] have reported ICS results for the combination of unresolved fine-structure levels, which include these particular levels. We compare our calculations for the combined transitions with these measurements and other theoretical results in Fig. 3. Note that the allowed transitions to the $2s_2$ and $2s_4$ dominate the cross sections when they are present and that although the measurements do not agree particularly well with the calculations when the transition to $3d_{11}$ is present, they do confirm the decrease with energy that is faster than expected for an allowed transition.

Our ICS results for the excitation of the $3p^5 5p$ manifold are displayed in Fig. 4. These cross sections show the expected energy dependence associated with the J_b values as discussed previously. Thus, the cross sections for excitation to the allowed $J_b = 0$ levels decrease more slowly than the ones for

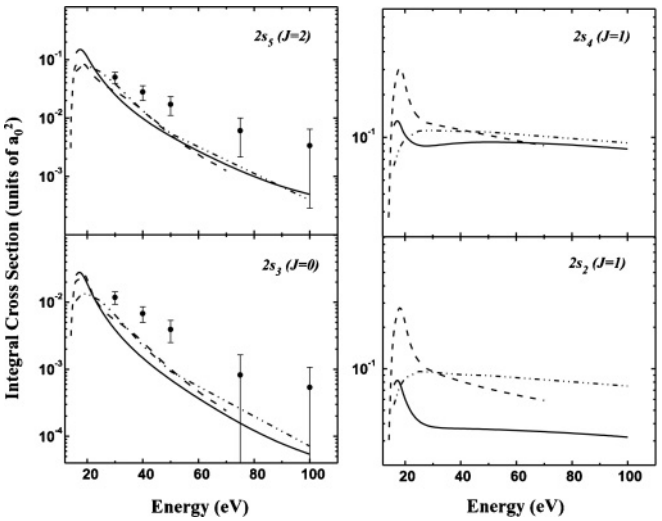

FIG. 2. Same as for Fig.1 for excitation of the $3p^5 5s$ levels except that the dashed line shows results disclosed in a private communication from Bartschat.

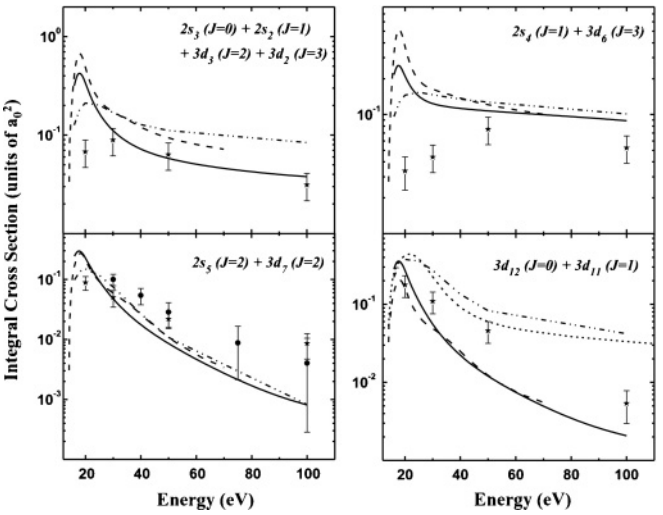

FIG. 3. Same as for Figs. 1 and 2 for unresolved excitations of certain $3p^5 3d$ and $3p^5 5s$ levels.

the $J_b = 2$ levels, whereas the cross sections for the forbidden transitions to levels with odd values of J_b fall off most rapidly. Weber *et al.* [9] do not report direct excitation cross sections for these transitions. The derived apparent cross sections shown in this article do have the expected qualitative behavior, but the ratio of the peak of the cross sections to the values at 100 eV is much larger than the ones we calculate, indicating there are substantial cascade effects at higher energies for which they have not corrected.

B. Differential cross sections

Chutjian and Cartwright [7] have measured the DCS for excitation to the $3p^5 3d$ and $3p^5 5s$ manifolds. In several cases where the energy of two or more fine-structure levels was very similar, they could not distinguish cross sections for the separate transitions and reported results for the combination. We have chosen to show these cases in Fig. 5 at impact energies of 30, 50, and 100 eV because they illustrate the various behaviors of the DCS as a function of the total angular momentum J_b of the excited levels.

In Fig. 5(a), we show the DCS for the excitation of the combined levels $2s_2$, $2s_3$, $3d_2$, and $3d_3$. These have J_b values of 1, 0, 3, and 2 respectively, thus displaying results for all possible J_b values. The results show most clearly the dependence of the magnitude of the DCS on J_b, especially at greater energies. Over most of the angular range, the dipole allowed transition to $2s_2$ dominates and exhibits the typical forward scattering peak. The transition to the $3d_2$ level with $J_b = 3$ is next in magnitude and has a much reduced forward peak, whereas the exchange transitions to the even levels have the smallest DCS and do not show a peak at forward scattering angles. Our combined cross sections agree very well with the experimental measurements, though these fall below our results in the midangular range at 30 eV. Note that the DCS for the transition to $3d_3$ increases steadily with the scattering angle and becomes the dominant cross section in the backward direction.

Figure 5(b) shows the DCS for the allowed dipole and octopole transition to the $2s_4$ and $3d_6$ levels having J_b

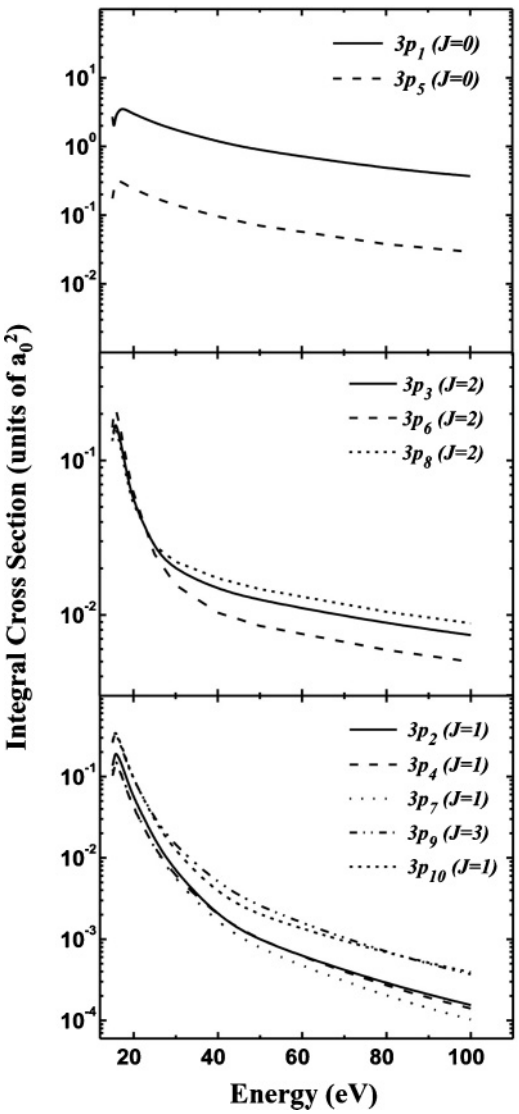

FIG. 4. Integrated cross sections in units of a_0^2 for the $3p^5 5p$ excitations.

values 1 and 3 respectively. Both cross sections show the typical forward peak with the dipole transition dominating the octopole one, except for larger scattering angles, where again the cross section for the $J_b = 3$ transition dominates in some scattering regions. There is good agreement with the measurements at 50 and 100 eV but not at 30 eV, where the measurements are much less than our results.

Figure 5(c) displays the DCS for the two forbidden transitions to the $2s_5$ and $3d_7$ levels, both with $J_b = 2$. These cross sections are relatively flat in the forward direction, contrary to the measurements, which show a pronounced forward peak. This implies that the measurements may be contaminated by a nearby strong allowed transition. Overall, the agreement with the experimental data is rather poor for these transitions. We also note that the DCS for the excitation of the $5s$ level has considerably more variation than the one for the $3d$ level.

Contamination of the measurements by nearby transitions as illustrated here would lead to incorrect extrapolated values and account in part for the disagreement between the

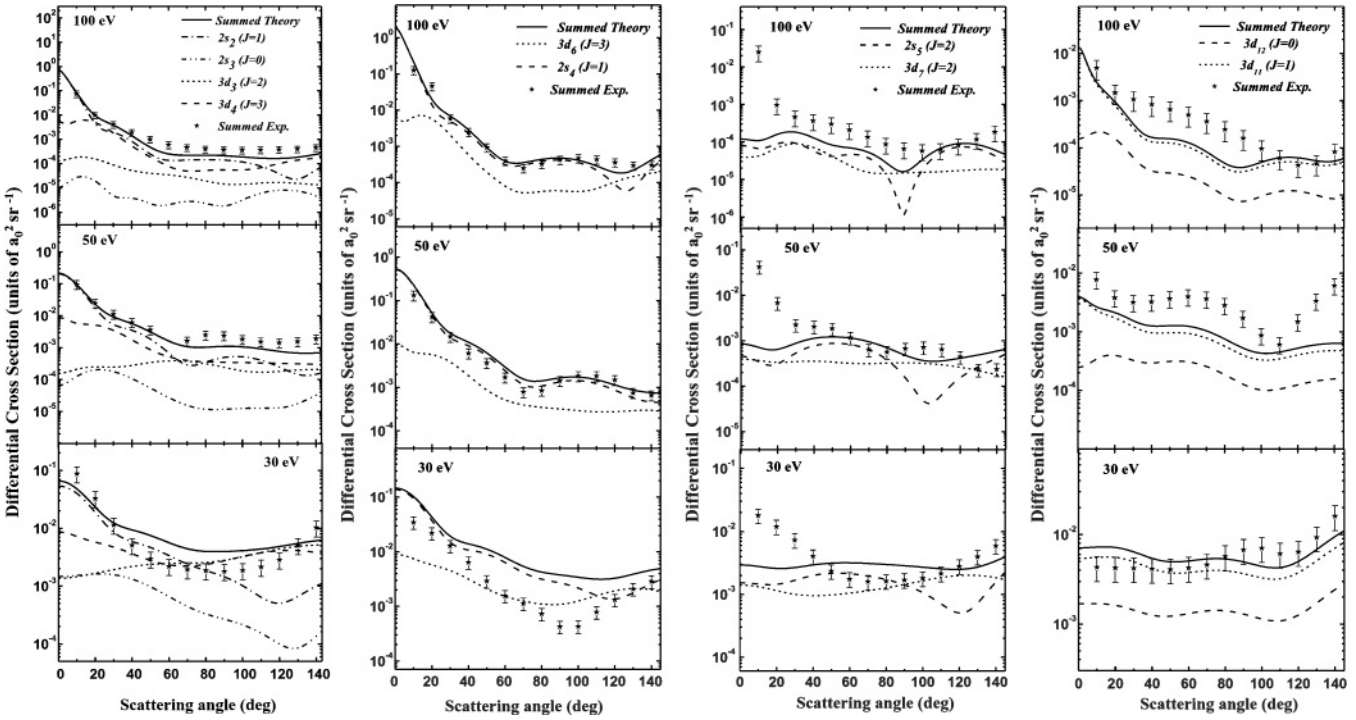

FIG. 5. Differential cross sections in units of a_0^2 sr^{-1} for (a) the unresolved combined levels $2s_2$, $2s_3$, $3d_2$, and $3d_3$; (b) the unresolved combined levels $2s_4$ and $3d_6$; (c) the unresolved combined levels $2s_5$ and $3d_7$; and (d) the unresolved combined levels $3d_{11}$ and $3d_{12}$.

ICS derived from these measurements and the theoretical calculations.

Finally, in Fig. 5(d), we show the results for the transitions to the dipole allowed $3d_{11}$ level and the forbidden $3d_{12}$ level having J_b values 1 and 0 respectively. In this case, the forward peak in the allowed transitions only appears as the incident energy increases. This is consistent with the fact that the ICS for excitation of the $3d_{11}$ level falls off more quickly than expected for an allowed transition and the expected behavior manifests itself only at greater energies, where the other contributions have decreased. The experimental measurements agree well with our results at 30 eV but deteriorate at greater energies.

Generally speaking, agreement with the experimental measurements is better for the allowed transitions, which have larger magnitudes. We have also calculated DCS for the excitation of the $3p^5 5p$ manifold but do not show these because there are no other results, either experimental or theoretical, with which to compare. The cross sections for the excitation of the allowed quadrupole levels with $J_b = 2$ show the expected strong forward peak but those for the allowed levels with $J_b = 0$ develop this peak only as the energy increases, similar to what was found for the $3d_{11}$ level. The DCS for the allowed levels with J_b even have considerably larger magnitudes in the forward directions than those with J_b odd.

C. Analytic fits to the integrated cross sections

The ICSs in units of a_0^2 for excitation of the allowed transitions to the $3p^5 3d$ and $3p^5 5s$ levels having a value of $J_b = 1$ are fitted by using the following equation:

$$\mathrm{ICS} = \frac{1}{E}[b_0 + b_1 \ln(E)]a_0^2. \tag{3}$$

Here, b_0 and b_1 are the fitting parameters. The energy E is in atomic units. We have used a form of Bethe-Born formula which does not explicitly include the optical oscillator strength because of the difference between the calculated and measured values. The fitted cross sections are valid for energies 30 eV and greater. The fitting parameters b_0 and b_1 for the different allowed excitations are given in Table IV. As noted previously, the cross section for excitation of the $3d_{11}$ level behaves like a forbidden transition rather than an allowed transition, as its J_b would indicate. This fitting is discussed next.

The ICSs, in units of a_0^2 for the forbidden transitions to the $3p^5 3d$ and $3p^5 5s$ manifolds with $J_b \neq 1$ as well as the parity forbidden transitions to the $3p^5 5p$ manifolds with all values of

TABLE IV. Fitting parameters b_0 and b_1 in Eq. (3) for the allowed transitions to the $3p^5 3d$ and $3p^5 5s$ manifolds.

Transition	b_0	b_1
$3d_1$ $(J = 1)$	0.567 93	1.289 80
$3d_5$ $(J = 1)$	0.194 18	0.429 65
$2s_4$ $(J = 1)$	0.841 12	0.166 31
$2s_2$ $(J = 1)$	0.028 54	0.067 84

TABLE V. Fitting parameters c_0 and c_1 in Eq. (4) for the forbidden transitions to the $3p^5 3d$, $3p^5 5s$, and $3p^5 5p$ manifolds.

Transition	c_0	c_1
$3d_2$ $(J=3)$	0.021 24	−1.063 58
$3d_3$ $(J=2)$	0.023 03	−3.160 34
$3d_4$ $(J=2)$	0.020 04	−3.163 39
$3d_6$ $(J=3)$	0.020 31	−0.940 35
$3d_7$ $(J=2)$	0.019 78	−3.178 91
$3d_8$ $(J=3)$	0.025 84	−1.153 73
$3d_9$ $(J=4)$	0.044 67	−2.975 57
$3d_{10}$ $(J=2)$	0.046 43	−2.944 98
$3d_{11}$ $(J=1)$	0.028 42	−2.159 72
$3d_{12}$ $(J=0)$	0.011 75	−2.835 73
$2s_5$ $(J=2)$	0.024 67	−3.034 75
$2s_3$ $(J=0)$	0.004 31	−3.381 75
$3p_1$ $(J=0)$	1.979 43	−1.310 53
$3p_2$ $(J=1)$	0.008 99	−3.272 91
$3p_3$ $(J=2)$	0.022 01	−0.867 07
$3p_4$ $(J=1)$	0.006 74	−3.029 69
$3p_5$ $(J=0)$	0.160 54	−1.332 14
$3p_6$ $(J=2)$	0.015 71	−0.909 74
$3p_7$ $(J=1)$	0.006 00	−3.195 55
$3p_8$ $(J=2)$	0.024 63	−0.804 54
$3p_9$ $(J=3)$	0.019 00	−3.114 03
$3p_{10}$ $(J=1)$	0.015 58	−2.984 14

J_b, are fitted using the following equation for energies greater than 30 eV:

$$\mathrm{ICS} = c_0 E^{c_1} a_0^2. \tag{4}$$

Here, c_0 and c_1 are the fitting parameters, and the values obtained for these parameters for the different forbidden transitions are given in Table V. As before, the energy E is in atomic units. From the results in Table V, we note the following patterns. For those forbidden transitions which have a nonzero direct contribution to the T matrix (J_b odd and not equal to unity for the $3p^5 3\,d$ and $3p^5 5\,s$ manifolds or J_b even for the $3p^5 5p$ manifold), the parameter c_1 is approximately equal to -1, whereas for the pure exchange transitions (J_b even for the $3p^5 3d$ and $3p^5 5\,s$ manifolds or J_b odd for the $3p^5 5p$ manifold), the parameter c_1 is approximately equal to -3. We have also fitted the cross section for the $3d_{11}$ level using Eq. (4) and included the coefficients in Table V. We note that in this case the exponent c_1 is close to -2, unlike any of the other fittings, reflecting its unique character.

IV. CONCLUSIONS

We have used our RDW method to calculate the cross sections for electron excitation from the ground state of argon to the fine-structure levels of the $3p^5 3d$, $3p^5 5s$, and $3p^5 5p$ manifolds at intermediate energies. These are compared to experimental results and previous calculations for both the integrated and differential cross sections. We have shown that these cross sections have the expected behavior as a function of the total angular momentum of the excited levels. As these data are important in plasma modeling studies, we have fitted the integrated cross sections with an analytic formula to enable the determination of these cross sections at arbitrary energies.

ACKNOWLEDGMENTS

This research was supported in part by a grant to ADS from Natural Sciences and Engineering Research Council of Canada (NSERC). RKG and RS are thankful to the Council of Scientific and Industrial Research, New Delhi, for financial support. LS acknowledges the support from the Helmholtz Gemeinschaft and Gesellschaft für Schwerionenforschung (GSI) (Nachwuchsgruppe VH-NG-421).

[1] J. B. Boffard, C. C. Lin, and C. A. DeJoseph, J. Phys. D **37**, R143 (2004).
[2] A. Hartgers, J. van Dijk, J. Jonkers, and J. A. M. van der Mullen, Comput. Phys. Commun. **135**, 199 (2001).
[3] E. Gargioni and B. Grosswendt, Rev. Mod. Phys. **80**, 451 (2008).
[4] S. Kaur, R. Srivastava, R. P. McEachran, and A. D. Stauffer, J. Phys. B **31**, 4833 (1998).
[5] R. Srivastava, A. D. Stauffer, and L. Sharma, Phys. Rev. A **74**, 012715 (2006).
[6] T. Zuo, R. P. McEachran, and A. D. Stauffer, J. Phys. B **24**, 2853 (1991).
[7] A. Chutjian and D. C. Cartwright, Phys. Rev. A **23**, 2178 (1981).
[8] J. E. Chilton and C. C. Lin, Phys. Rev. A **60**, 3712 (1999).
[9] T. Weber, J. B. Boffard, and C. C. Lin, Phys. Rev. A **68**, 032719 (2003).
[10] V. E. Bubelev and A. M. Grum-Grzhimailo, J. Phys. B **24**, 2183 (1991).
[11] D. H. Madison, A. Dasgupta, K. Bartschat, and D. Vaid, J. Phys. B **37**, 1073 (2004).
[12] K. Bartschat and V. Zeman, Phys. Rev. A **59**, R2552 (1999).
[13] F. A. Parpia, C. F. Fischer, and I. P. Grant, Comput. Phys. Commun. **94**, 249 (1996).
[14] A. Dasgupta, J. P. Apruzese, O. Zatsarinny, K. Bartschat, and C. Froese Fischer, Phys. Rev. A **74**, 012509 (2006).
[15] Yu. Ralchenko, A. E. Kramida, J. Reader, and the NIST ASD team, NIST Atomic Spectra Database (version 3.1.5) (National Institute of Standards and Technology, Gaithersburg, MD, 2010), [http://physics.nist.gov/asd3].